

Phase diagram of the J_1 - J_2 Heisenberg second-order topological quantum magnet

Pascal M. Vecsei¹ and Jose L. Lado¹

¹*Department of Applied Physics, Aalto University, 00076 Aalto, Finland*

(Dated: August 30, 2024)

Competing interactions in quantum magnets lead to a variety of emergent states, including ordered phases, nematic magnets and quantum spin liquids. Among them, topological quantum magnets represent a promising platform to create topological excitations protected by the bulk many-body excitation gap. Here we establish the phase diagram of a breathing frustrated antiferromagnetic J_1 - J_2 -Heisenberg model, featuring both ordered states and a higher-order topological quantum magnet state. Using exact many-body methods based on neural network quantum states and tensor networks, we determine the existence of a first order phase transition between stripe order and the topological quantum magnet and the second order phase transition between the Néel order and quantum magnet phase, further corroborated by calculations of the many-body gap. Using an auxiliary fermion parton formalism, we show the emergence of topological spinon corner modes stemming from the breathing order parameter of the parent Heisenberg model. Our results establish the breathing frustrated square lattice Heisenberg model as a paradigmatic system to engineer topological quantum magnetism, as recently realized in Ti lattices at MgO.

Quantum magnets[1, 2] represent one of the most exotic states of matter in condensed matter physics. Frustrated magnetism is a fertile platform to give rise to unconventional excitations, including magnons[3, 4], spinons[5], triplons[6, 7], visons[8] and gauge excitations. Models of quantum magnets have attracted much attention[9], in particular with regards to the different unconventional phases that may appear in their phase diagram. Frustrated Heisenberg models often have a variety of competing phases, including spin liquid[10–14], stripe and zigzag antiferromagnetic[15–18], valence bond states[19–22], and spin spiral phases[23, 24]. A variety of natural material host potentially frustrated spin models, including RuCl₃[25–30], 1T-TaS₂[31–34], FeSe[35, 36] and Herbertsmithite[37–41] are among some of the proposed materials that may host a variety of competing magnetic states driven by frustration and quantum fluctuations.

Beyond naturally occurring materials, artificial platforms based on atomically precise manipulation have risen as an alternative to create artificial quantum magnets with highly controllable interactions[42–44]. Atomically engineered quantum magnets with scanning tunneling microscopy allowed to create models of magnetic criticality[45], magnets featuring magnon[46], triplon[7, 47] and spinon excitations[48–51], and first order and second order topological quantum magnets[47, 52, 53]. Such many-body symmetry protected topological phases represent one of the frontiers in topological matter[54–66]. In particular, the robustness and nature of the recently realized second order topological quantum magnet[53] remains an open problem in quantum magnetism.

In this Letter we establish the phase diagram of the first higher-order topological magnet realized experimentally, which consists of a frustrated breathing square lattice $J_1 - J_2$ Heisenberg model. We demonstrate the existence of three widely different regions, including a Néel

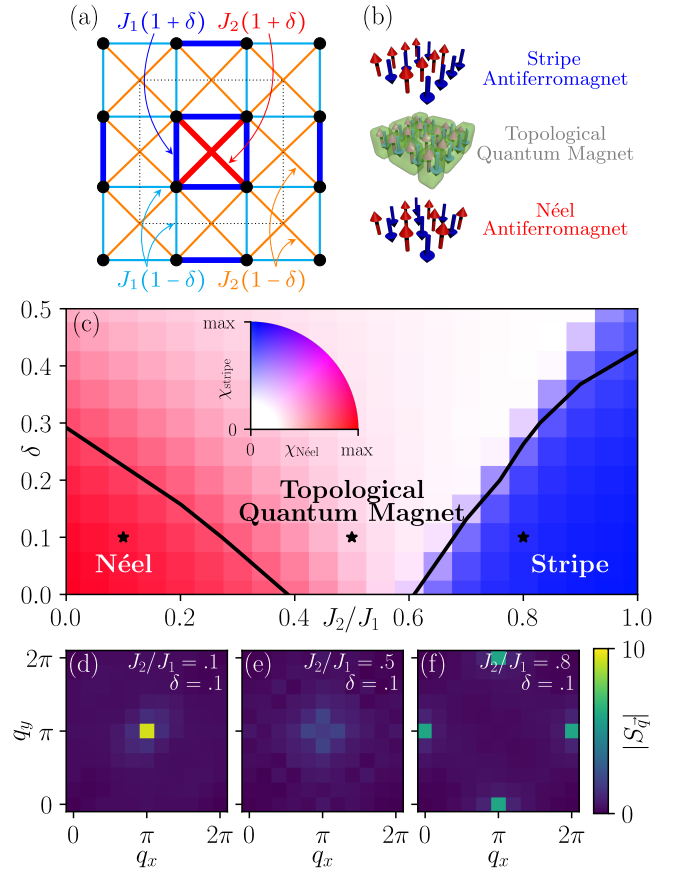


FIG. 1. (a,b) Schematic of the breathing $J_1 - J_2$ Heisenberg model, featuring three phases including Néel, stripe and Dirac quantum magnet. Panel (c) shows the phase diagram, where the background shows the Néel as red and the stripe order parameters as blue. The lines indicate the phase transition, as obtained using neural network quantum states. Panels (d-f) show the spin structure factor at the marked stars in (c).

ordered regime, a stripe antiferromagnetic region, and a

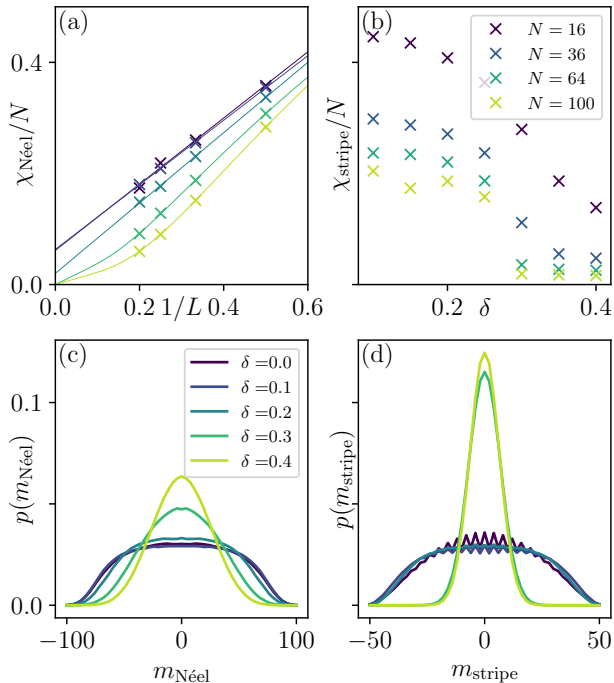


FIG. 2. Behavior of the magnetization with increasing system size and breathing δ . Panel (a) shows the second moment of the Néel magnetization as function of δ and system size $N = 4L^2$ for fixed $J_2 = 0.1$. An extrapolation of form $a/L + be^{-cL}$ is used to estimate the value in the thermodynamic limit, where $c = 0$ if a linear extrapolation yields a positive b . Panel (c) shows the distribution of the magnetization for fixed $N = 100$. The stripe order phase transition at fixed $J_2 = 0.8$ is treated in panels (b,d). Panel (b) shows the squared stripe order parameter as function of δ , for the different system sizes. A clear jump can be seen between $\delta = 0.25$ and $\delta = 0.3$. This jump is also reflected in a sudden change in the magnetization distribution, as shown in panel (d).

gapped topological quantum magnet as realized experimentally. Our phase diagram is demonstrated using a combination of exact quantum many-body methods based on tensor-networks and neural-network quantum states, which allows to trace out the phase diagram both using susceptibilities and quantum many-body gaps. Using an auxiliary fermion formalism we further show how the exact many-body results are related to the low energy spinon model of the topological quantum magnet. Our results establish the phase diagram of a paradigmatic model featuring topological quantum magnetism, establishing the required groundwork to study exotic phenomena in a realistic system featuring higher-order topological quantum many-body matter.

Model: In the following, we study a breathing antiferromagnetic Heisenberg model on a square lattice with first and second neighbor interactions as realized in Ti at

MgO lattices[53, 67–69]. The Hamiltonian is

$$\hat{\mathcal{H}} = \sum_{ij} J_{ij} \vec{S}_i \cdot \vec{S}_j, \quad (1)$$

where J_{ij} are the interactions and $\vec{S}_i = (S_i^x, S_i^y, S_i^z)$ are the spin operators used to represent the local spin-1/2 operators as $S_i^k = \sigma_i^k/2$. The relative strength of the interactions is depicted in Fig. 1(a). The model consists of square plaquettes within which the interactions are strong, while between different plaquettes the interaction is weak. The unit cell is indicated by a thin dotted line in Fig. 1(a), and couplings of different strength are marked with different colors. By setting $\delta = 0$, we recover the well-known square lattice J_1 - J_2 antiferromagnetic Heisenberg model. At zero breathing $\delta = 0$, signatures of a valence bond solid phase (VBS) for $J_2/|J_1| \lesssim 0.6$, and a potential gapless Dirac spin-liquid in a region $0.49 \lesssim J_2/|J_1| \lesssim 0.54$ have attracted many efforts[70–75]. Here we map out the phase diagram for finite breathing $\delta > 0$ as recently realized in experiment[53], further showing how its low energy description is linked to the previous phases at $\delta = 0$. This quantum magnet realizes a topological phase featuring a topological degeneracy associated with gapless corner excitations. We show that the low energy Hamiltonian can be described with an auxiliary fermion formalism whose effective parameters can be extracted from our many-body calculations.

Variational many-body formalism: We solve two-dimensional many-body spin models of up to 100 quantum spins with periodic boundary conditions using Neural Network Quantum States (NNQS)[76] and matrix product states (MPS)[77]. The neural network quantum states we used are group convolutional neural networks (GCNN), which deliver high-accuracy ground states for frustrated models[78, 79]. The GCNN we used are 10 layers deep and have 10 filters per layer. They are fully symmetric under parity and the space group symmetries of the lattice, which has, compared to the square lattice model at $\delta = 0$, a reduced translational symmetry. The nets have up to 361100 complex parameters for $N = 100$ spin sites. The wave functions were optimized using an efficient stochastic reconfiguration algorithm[80–82][83]. MPS calculations are performed with a maximum bond dimension $\chi_m = 1000$, wavefunctions are optimized with the density matrix renormalization algorithm[84] using quantum number conservation[85].

Phase Diagram: We distinguish between three wide phases (cf. Fig. 1(b)): a Néel antiferromagnetic for small J_2 and δ , an intermediate topological quantum magnet phase, and a stripe order antiferromagnetic phase for large J_2 and small δ . The order parameters to distinguish between these three phases are defined through the operators

$$\hat{M}_{\text{Néel/stripe}} = \sum_{\vec{\alpha}} \zeta_{\vec{\alpha}} \hat{S}_{\vec{\alpha}}^z, \quad (2)$$

where the sum runs over the two dimensional indices $\vec{\alpha} = (i, j)$, and $\zeta_{\vec{\alpha}} = 2(-1)^i(-1)^j$ for the Néel order parameter and $\zeta_{\vec{\alpha}} = ((-1)^i + (-1)^j)$ for the stripe order parameter. As the model is time reversal symmetric, the first moment of these order parameters vanishes. The second moment reflects the Néel and stripe susceptibilities, and allows us to distinguish ordered and disordered phases. The resulting phase diagram is shown in Fig. 1(c) as the solid black lines, where the background showing the Néel and stripe magnetic susceptibilities for a 36 spin system obtained from matrix product state calculations with periodic boundary conditions. We show in Fig 1(d)-(f) the spin structure factor $S(\vec{q}) = 4 \sum_{\vec{\alpha}\vec{\beta}} e^{-i\vec{\beta}\cdot\vec{q}/2L} \langle \vec{S}_{\vec{\alpha}} \cdot \vec{S}_{\vec{\alpha}+\vec{\beta}} \rangle / N$ for the three points marked with stars in Fig. 1(c). Panel Fig 1(d) is located well within the Néel phase, featuring a clear peak at $(q_x, q_y) = (\pi, \pi)$ signaling the Néel order. Fig 1(e) is located within the quantum magnet phase, and the magnetic structure factor shows no clear peak. The stripe order antiferromagnet is shown in panel Fig 1(f), featuring peaks at the locations $(q_x, q_y) = (\pi, 0)$ and $(0, \pi)$ as expected from a stripe phase.

To locate the phase transition, we study the magnetization as a function of system size, breathing δ and next-to-nearest neighbor exchange J_2 . In Fig. 2(a), we show the second moment of the magnetization, which increases as we move into the symmetry broken Néel antiferromagnetic phase, for fixed $J_2 = 0.1$. We evaluate this quantity from our numerical calculations for differently sized finite clusters, and then extrapolate linearly to the thermodynamic limit. A non-zero extrapolated value of $\chi_{\text{Néel}}/N = \langle M_{\text{Néel}}^2 \rangle / N^2$ implies that the susceptibility $\chi_{\text{Néel}} = \langle M_{\text{Néel}}^2 \rangle / N$ diverges, as expected at the phase transition. In Fig. 2(c) we show the distribution of the Néel magnetization for $J_2 = 0.1$ and variable δ for fixed system size $N = 100$ quantum spins. It is defined as $p(m_{\text{Néel/stripe}}) = \langle \psi | P_{m_{\text{Néel/stripe}}} | \psi \rangle / \langle \psi | \psi \rangle$, where $P_{m_{\text{Néel/stripe}}}$ is the projector into the eigenspace of $\hat{M}_{\text{Néel/stripe}}$ with eigenvalue $m_{\text{Néel/stripe}}$. While for large δ , in the quantum magnet phase, this distribution is Gauss-like in shape and clearly peaked at $m_{z,\text{Néel}} = 0$, as the breathing decreases the distributions becomes wider. This phase transition from the quantum magnet to the Néel antiferromagnetic phase shows the typical behavior of a second order phase transition, with a continuous change in the order parameter for finite system sizes.

Next, let us study the transition into the stripe-antiferromagnetic phase. There, we encounter a first order phase transition, which is signaled by a rapid change in the magnetization. This can be also observed as a kink in the ground state energy, a change in the degeneracy of the ground state already on finite clusters, and a change in the symmetry of the lowest $S_z = 1$ state. The sudden change in the magnetization is reflected in the second moment, which is shown in Fig. 2(b) as a function of δ and system size. For large system sizes, there is a clear

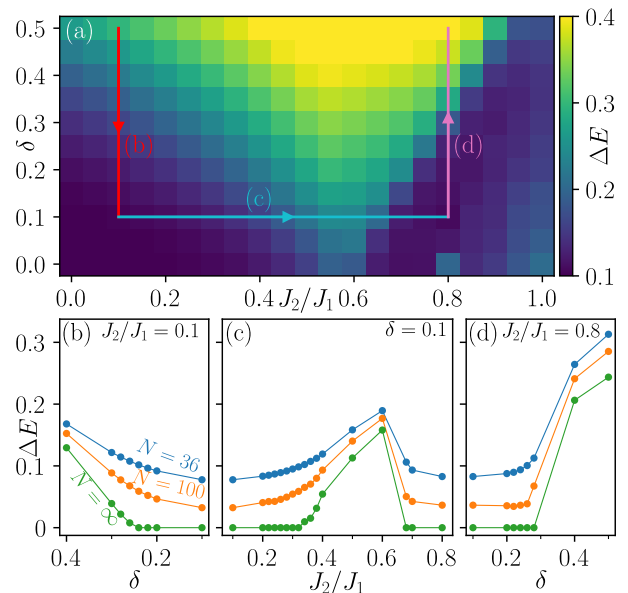


FIG. 3. The background color in panel (a) shows the gap between the lowest $S_z = 1$ state and the ground state, from $N = 36$ system by MPS. We clearly see two regions with low gap, which are the Néel and the stripe phase regions, both of which have gapless magnons. The gap along the path depicted in panel (a) is shown in panels (b)-(d), with data obtained from NNQS and a linear extrapolation of these two data points.

jump in this quantity at the phase transition, which allows us to locate the phase transition. In Fig. 2(d), we show the stripe magnetization distribution for $J_2/J_1 = 0.8$ for varying δ . While for large δ , in the quantum magnet phase, the distribution is strongly peaked at around zero, it suddenly becomes much wider as we pass through the phase transition.

Phase transition from many-body gaps: In the antiferromagnetic phases, both the Néel and the stripe order, gapless magnons exist above the ground state. In contrast, in the topological quantum magnet phase for $\delta > 0$ with closed boundary conditions, the system features a finite gap in the thermodynamic limit. The transition between those states can be detected by looking for a closing of the gap between the ground state and the $S_z = 1$ excitations. To do this, we map out the gap between the $S_z = 0$ and $S_z = 1$ sectors for a $N = 36$ spin system, as shown in Fig. 3(a). We see two regions with a clearly smaller gap, corresponding to the Néel and stripe antiferromagnet. To obtain more detailed information, we study the gap with NNQS along the path shown in Fig. 3(a). Fig. 3(b) shows the vertical section for fixed $J_2 = 0.1$, passing from the topological quantum magnet to the Néel ordered phase. We show the gap for system sizes $N = 36$ and $N = 100$, as well as a power law extrapolation to the thermodynamic limit[86]. As δ decreases, so does the size of the gap, which eventually reaches zero

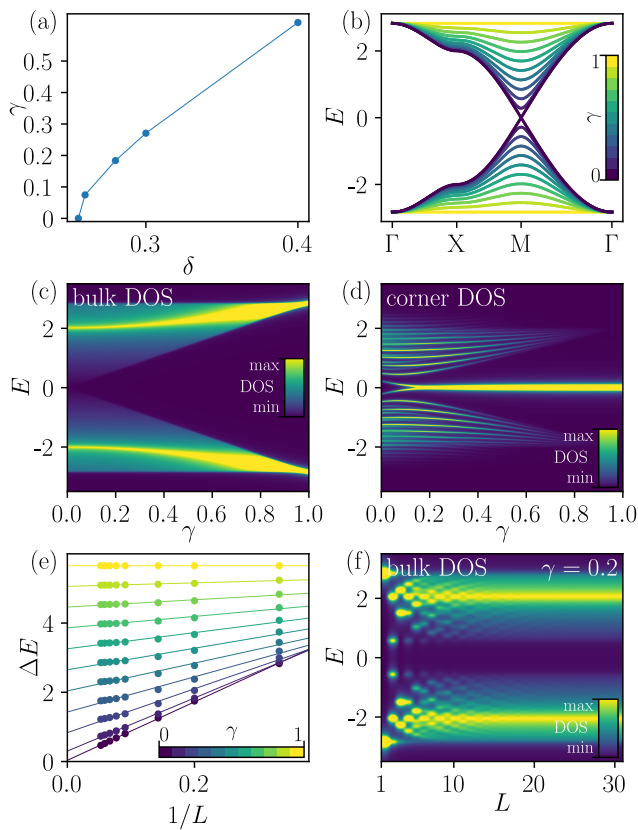


FIG. 4. Plots about the corresponding spinon model. Panel (a) shows the mapping between γ and δ for fixed $J_2 = 0.1$, as obtained by the assumption that the equivalent values have the same ratio $\Delta E_{L=5}/\Delta E_{L=3}$. Panel (b) shows the band structure as function of the breathing γ . Panel (c) shows the DOS for infinite systems, as function of dimerization γ . The corner DOS for finite systems of size 20×20 is shown in panel (d) as function of γ . Panel (e) shows the size-dependent gap size for different values of γ , with a linear extrapolation. Panel (b) shows the the bulk DOS for finite sized periodic systems as function of the size.

at a value of δ in good agreement with the results from the magnetization calculations. Fig. 3(c) shows the gap along the horizontal path, at fixed $\delta = 0.1$. For $J_2 < 0.5$, the gap first stays zero and then increases as the system passes from the Néel ordered into the topological quantum magnet phase. Eventually, as the system transitions into the stripe ordered phase, it becomes gapless again. Fig. 3(d) shows the evolution of the gap along the fixed line at $J_2 = 0.8$. The energies of the excited states were obtained by looking for the lowest energy state at finite S_z . [87]

Auxiliary pseudofermion representation: In the quantum disordered regime, the Heisenberg Hamiltonian $H = \sum_{ij} J_{ij} \vec{S}_i \cdot \vec{S}_j$ can be approximately solved using with auxiliary Abrikosov fermions [88–91] $\vec{S}_n = \frac{1}{2} \sum_{s,s'} \vec{\sigma}_{s,s'} f_{n,s}^\dagger f_{n,s'}$ with the constraint $\sum_s f_{n,s}^\dagger f_{n,s} = \mathcal{I}$.

Using the replacement in the Heisenberg Hamiltonian and performing a saddle point approximation in the effective action gives rise to the effective spinon Hamiltonian

$$\mathcal{H} = \sum_{ij} \Gamma_{ij} f_{i,s}^\dagger f_{j,s}, \quad (3)$$

where the spinon hoppings give rise to a π -flux model $\prod_{ij} \text{sign}(\Gamma_{ij}) = -1$ around each plaquette, and $\Gamma_{ij} = \Gamma_0(1 \pm \gamma)$ featuring a first neighbor breathing analogous to Fig. 1a. The previous Hamiltonian with $\gamma = 0$ describes the gapless Dirac spin liquid [71, 73] of the J_1 - J_2 Heisenberg model, featuring gapless Dirac spinons. The breathing order parameter γ opens a gap in the spinon spectra, leading to a state analogous to the plaquette bond ordered phase [19, 21, 22, 71, 92]. Within this model, the gapless Dirac spin liquid state of the square lattice corresponds to the limit $\gamma = 0$, whereas the plaquette ordering stems from a dynamically generated Dirac mass leading to $\gamma \neq 0$. The topological nature of the spin many-body breathing phase can be understood in terms of the topological classification arising from the combination of time reversal symmetry \mathcal{T} with one of the point group symmetries, diagonal reflection R_{xy} or C_4 rotation [54–56]. The combination of these symmetries imposes a topological classification onto the space of many-body gapped bosonic Hamiltonians with spin 1/2. The nontrivial phase, which arises for $\delta < 0$, has topological corner modes with spin 1/2, and is referred to as higher-order symmetry protected topological phase [54]. For $\delta > 0$ we encounter the corresponding trivial phase for which all of the sites are translated diagonally by one site. In this gapped phase, the system becomes topologically nontrivial as can be evaluated using the nested Wilson loop of the effective spinon Hamiltonian [93–96], and leading to topological spinon corner modes.

The parameters of the effective spinon model can be extracted by comparing the many-body gaps of the exact quantum many-body calculations with those of the effective model. In particular, we compare the ratio of the gap sizes between systems with $L = 5$ and $L = 3$, $\Delta E_{L=5}/\Delta E_{L=3}$ between the spinon model and the numerical results for the Heisenberg model at $\delta = 0.1$. This allows us to obtain a mapping between the breathing parameter of the spinon model γ , and the corresponding breathing parameter of the Heisenberg model, δ , as shown in Fig. 4(a). When the breathing becomes non-zero in the effective model, Dirac spinons develop a mass leading to gapped excitations, as depicted in Fig. 4(b). Fig. 4(c) shows the spinon DOS for the infinite system in the bulk. The corner spinon DOS is shown in Fig. 4(d), where a zero mode can be clearly seen for large enough breathing. The gap in the thermodynamic limit can be obtained from an extrapolation from small systems in Fig. 3(e), in analogy to our exact quantum many-body calculations. It is worth noting that the extrapolation fol-

lows the linear dependence expected from gapped Dirac spinons for small dimerization, as shown in Fig. 4(e). This phenomenology can be directly observed by computing the bulk spinon DOS as a function of the system size at fixed $\gamma = 0.2$ as shown in Fig. 4 (f), showing the decrease and saturation of the gap.

Conclusion Frustration in quantum many-body systems is a recognized driving force for unconventional phenomena. Here, we have presented the phase diagram of a J_1 - J_2 Heisenberg model on a breathing square lattice, a recently experimentally realized model in Ti atoms on MgO featuring topological corner modes. Using exact many-body methods based on large-scale tensor network and neural network quantum state calculations, we have mapped out its magnetic phase diagram, revealing the phase boundaries between the Néel antiferromagnetic, the topological quantum magnet and the stripe-antiferromagnetic phases. This phase diagram contains a region with a topological quantum magnet phase, sharing a first order phase transition to the stripe order and a second order phase transition to the Neel state. Furthermore, using an auxiliary fermion formalism we have mapped the results of our many-body methods to a gapped quantum spinon model, revealing the evolution of the topological bulk gap and topological corner modes in this model. Our findings put forward a rich phase diagram of a model realizing topological quantum magnetism as recently demonstrated experimentally with Ti atoms at MgO. Our results establish a paradigmatic system to explore topological phases in frustrated breathing Heisenberg models, and their connection to gapped and gapless spinon phases through neural network and tensor network many-body methods.

Acknowledgements We thank C. Flindt, M. Niedermeier, K. Yang, S. Dominguez and T. Antao for useful discussions. We acknowledge the computational resources provided by the Aalto Science-IT project and CSC (Finland) for awarding this project access to the LUMI supercomputer, owned by the EuroHPC Joint Undertaking, hosted by CSC (Finland) and the LUMI consortium. We acknowledge the support from the Research Council of Finland through grants (Grants No. 331342 and No. 358088), the Finnish Quantum Flagship, and the Finnish Centre of Excellence in Quantum Technology (Project No. 312299), and the Jane and Aatos Erkko Foundation.

[1] L. Savary and L. Balents, Quantum spin liquids: a review, *Reports on Progress in Physics* **80**, 016502 (2016).
 [2] Y. Zhou, K. Kanoda, and T.-K. Ng, Quantum spin liquid states, *Rev. Mod. Phys.* **89**, 025003 (2017).
 [3] R. Coldea, D. A. Tennant, K. Habicht, P. Smeibidl, C. Wolters, and Z. Tylczynski, Direct Measurement of the Spin Hamiltonian and Observation of Condensa-

tion of Magnons in the 2d Frustrated Quantum Magnet Cs_2CuCl_4 , *Phys. Rev. Lett.* **88**, 137203 (2002).
 [4] J. Schulenburg, A. Honecker, J. Schnack, J. Richter, and H.-J. Schmidt, Macroscopic Magnetization Jumps due to Independent Magnons in Frustrated Quantum Spin Lattices, *Phys. Rev. Lett.* **88**, 167207 (2002).
 [5] W. Ruan, Y. Chen, S. Tang, J. Hwang, H.-Z. Tsai, R. L. Lee, M. Wu, H. Ryu, S. Kahn, F. Liou, C. Jia, A. Aikawa, C. Hwang, F. Wang, Y. Choi, S. G. Louie, P. A. Lee, Z.-X. Shen, S.-K. Mo, and M. F. Crommie, Evidence for quantum spin liquid behaviour in single-layer 1T-TaSe₂ from scanning tunnelling microscopy, *Nature Physics* **17**, 1154–1161 (2021).
 [6] Y. Chen, M. Sato, Y. Tang, Y. Shiomi, K. Oyanagi, T. Masuda, Y. Nambu, M. Fujita, and E. Saitoh, Triplon current generation in solids, *Nature Communications* **12**, 10.1038/s41467-021-25494-7 (2021).
 [7] R. Drost, S. Kezilebieke, J. L. Lado, and P. Liljeroth, Real-Space Imaging of Triplon Excitations in Engineered Quantum Magnets, *Phys. Rev. Lett.* **131**, 086701 (2023).
 [8] Y. Huh, M. Punk, and S. Sachdev, Vison states and confinement transitions of \mathbb{Z}_2 spin liquids on the kagome lattice, *Phys. Rev. B* **84**, 094419 (2011).
 [9] W. Ye and L. Zou, Classification of Symmetry-Enriched Topological Quantum Spin Liquids, *Phys. Rev. X* **14**, 021053 (2024).
 [10] Z. Zhu and S. R. White, Spin liquid phase of the $s = \frac{1}{2}$ $J_1 - J_2$ Heisenberg model on the triangular lattice, *Phys. Rev. B* **92**, 041105 (2015).
 [11] S. Depenbrock, I. P. McCulloch, and U. Schollwöck, Nature of the Spin-Liquid Ground State of the $s = 1/2$ Heisenberg Model on the Kagome Lattice, *Phys. Rev. Lett.* **109**, 067201 (2012).
 [12] S. Yan, D. A. Huse, and S. R. White, Spin-Liquid Ground State of the $S = 1/2$ Kagome Heisenberg Antiferromagnet, *Science* **332**, 1173–1176 (2011).
 [13] S. Hu, W. Zhu, S. Eggert, and Y.-C. He, Dirac Spin Liquid on the Spin-1/2 Triangular Heisenberg Antiferromagnet, *Phys. Rev. Lett.* **123**, 207203 (2019).
 [14] A. Szasz, J. Motruk, M. P. Zaletel, and J. E. Moore, Chiral Spin Liquid Phase of the Triangular Lattice Hubbard Model: A Density Matrix Renormalization Group Study, *Phys. Rev. X* **10**, 021042 (2020).
 [15] H. Li, H.-K. Zhang, J. Wang, H.-Q. Wu, Y. Gao, D.-W. Qu, Z.-X. Liu, S.-S. Gong, and W. Li, Identification of magnetic interactions and high-field quantum spin liquid in α - RuCl_3 , *Nature Communications* **12**, 10.1038/s41467-021-24257-8 (2021).
 [16] S. M. Winter, Y. Li, H. O. Jeschke, and R. Valentí, Challenges in design of Kitaev materials: Magnetic interactions from competing energy scales, *Phys. Rev. B* **93**, 214431 (2016).
 [17] A. Baum, H. N. Ruiz, N. Lazarević, Y. Wang, T. Böhm, R. Hosseinian Ahangharnejhad, P. Adelman, T. Wolf, Z. V. Popović, B. Moritz, T. P. Devereaux, and R. Hackl, Frustrated spin order and stripe fluctuations in FeSe, *Communications Physics* **2**, 10.1038/s42005-019-0107-y (2019).
 [18] P. A. Maksimov and A. L. Chernyshev, Rethinking α - RuCl_3 , *Phys. Rev. Res.* **2**, 033011 (2020).
 [19] F. Ferrari and F. Becca, Gapless spin liquid and valence-bond solid in the J_1 - J_2 Heisenberg model on the square lattice: Insights from singlet and triplet excitations, *Phys. Rev. B* **102**, 014417 (2020).

- [20] S.-S. Gong, W. Zhu, D. N. Sheng, O. I. Motrunich, and M. P. A. Fisher, Plaquette Ordered Phase and Quantum Phase Diagram in the Spin- $\frac{1}{2}$ J_1 - J_2 Square Heisenberg Model, *Phys. Rev. Lett.* **113**, 027201 (2014).
- [21] L. Wang and A. W. Sandvik, Critical Level Crossings and Gapless Spin Liquid in the Square-Lattice Spin-1/2 J_1 - J_2 Heisenberg Antiferromagnet, *Phys. Rev. Lett.* **121**, 107202 (2018).
- [22] J. Huang, X. Qian, and M. Qin, Is the Valence Bond Solid state in J_1 - J_2 Square Lattice Heisenberg Model Plaquette or Columnar?, *arXiv e-prints*, arXiv:2406.17417 (2024), arXiv:2406.17417 [cond-mat.str-el].
- [23] L. Capriotti, A. E. Trumper, and S. Sorella, Long-Range Néel Order in the Triangular Heisenberg model, *Phys. Rev. Lett.* **82**, 3899 (1999).
- [24] R. Suttner, C. Platt, J. Reuther, and R. Thomale, Renormalization group analysis of competing quantum phases in the J_1 - J_2 Heisenberg model on the kagome lattice, *Phys. Rev. B* **89**, 020408 (2014).
- [25] A. Banerjee, J. Yan, J. Knolle, C. A. Bridges, M. B. Stone, M. D. Lumsden, D. G. Mandrus, D. A. Tennant, R. Moessner, and S. E. Nagler, Neutron scattering in the proximate quantum spin liquid RuCl₃, *Science* **356**, 1055 (2017).
- [26] T. Yokoi, S. Ma, Y. Kasahara, S. Kasahara, T. Shibauchi, N. Kurita, H. Tanaka, J. Nasu, Y. Motome, C. Hickey, S. Trebst, and Y. Matsuda, Half-integer quantized anomalous thermal Hall effect in the Kitaev material candidate RuCl₃, *Science* **373**, 568 (2021).
- [27] P. Czaika, T. Gao, M. Hirschberger, P. Lampen-Kelley, A. Banerjee, J. Yan, D. G. Mandrus, S. E. Nagler, and N. P. Ong, Oscillations of the thermal conductivity in the spin-liquid state of α -RuCl₃, *Nature Physics* **17**, 915–919 (2021).
- [28] B. Yang, Y. M. Goh, S. H. Sung, G. Ye, S. Biswas, D. A. S. Kaib, R. Dhakal, S. Yan, C. Li, S. Jiang, F. Chen, H. Lei, R. He, R. Valentí, S. M. Winter, R. Hovden, and A. W. Tsen, Magnetic anisotropy reversal driven by structural symmetry-breaking in monolayer α -RuCl₃, *Nature Materials* **22**, 50–57 (2022).
- [29] Y.-F. Jiang, T. P. Devereaux, and H.-C. Jiang, Field-induced quantum spin liquid in the Kitaev-Heisenberg model and its relation to α -RuCl₃, *Phys. Rev. B* **100**, 165123 (2019).
- [30] L. Janssen, S. Koch, and M. Vojta, Magnon dispersion and dynamic spin response in three-dimensional spin models for α -RuCl₃, *Phys. Rev. B* **101**, 174444 (2020).
- [31] K. T. Law and P. A. Lee, 1T-TaS₂ as a quantum spin liquid, *Proceedings of the National Academy of Sciences* **114**, 6996–7000 (2017).
- [32] S. Mañas-Valero, B. M. Huddart, T. Lancaster, E. Coronado, and F. L. Pratt, Quantum phases and spin liquid properties of 1T-TaS₂, *npj Quantum Materials* **6**, 10.1038/s41535-021-00367-w (2021).
- [33] S. Pal and S. Roy, Understanding the magnetic response of the Quantum Spin Liquid compound 1T-TaS₂, *Physica B: Condensed Matter* **643**, 414121 (2022).
- [34] C.-K. Li, X.-P. Yao, J. Liu, and G. Chen, Fractionalization on the Surface: Is Type-II Terminated 1T-TaS₂ Surface an Anomalously Realized Spin Liquid?, *Phys. Rev. Lett.* **129**, 017202 (2022).
- [35] J.-H. She, M. J. Lawler, and E.-A. Kim, Quantum Spin Liquid Intertwining Nematic and Superconducting Order in FeSe, *Phys. Rev. Lett.* **121**, 237002 (2018).
- [36] S.-S. Gong, W. Zhu, D. N. Sheng, and K. Yang, Possible nematic spin liquid in spin-1 antiferromagnetic system on the square lattice: Implications for the nematic paramagnetic state of FeSe, *Phys. Rev. B* **95**, 205132 (2017).
- [37] M. R. Norman, Colloquium: Herbertsmithite and the search for the quantum spin liquid, *Rev. Mod. Phys.* **88**, 041002 (2016).
- [38] D. E. Freedman, T. H. Han, A. Prodi, P. Müller, Q.-Z. Huang, Y.-S. Chen, S. M. Webb, Y. S. Lee, T. M. McQueen, and D. G. Nocera, Site Specific X-ray Anomalous Dispersion of the Geometrically Frustrated Kagomé Magnet, Herbertsmithite, ZnCu₃(OH)₆Cl₂, *Journal of the American Chemical Society* **132**, 16185–16190 (2010).
- [39] T.-H. Han, M. R. Norman, J.-J. Wen, J. A. Rodriguez-Rivera, J. S. Helton, C. Broholm, and Y. S. Lee, Correlated impurities and intrinsic spin-liquid physics in the kagome material herbertsmithite, *Phys. Rev. B* **94**, 060409 (2016).
- [40] D. Wulferding, P. Lemmens, P. Scheib, J. Röder, P. Mendels, S. Chu, T. Han, and Y. S. Lee, Interplay of thermal and quantum spin fluctuations in the kagome lattice compound herbertsmithite, *Phys. Rev. B* **82**, 144412 (2010).
- [41] C. Zhang and T. Li, Variational study of the ground state and spin dynamics of the spin- $\frac{1}{2}$ kagome antiferromagnetic Heisenberg model and its implication for herbertsmithite ZnCu₃(OH)₆Cl₂, *Phys. Rev. B* **102**, 195106 (2020).
- [42] D.-J. Choi, N. Lorente, J. Wiebe, K. von Bergmann, A. F. Otte, and A. J. Heinrich, Colloquium: Atomic spin chains on surfaces, *Rev. Mod. Phys.* **91**, 041001 (2019).
- [43] A. A. Khajetoorians, D. Wegner, A. F. Otte, and I. Swart, Creating designer quantum states of matter atom-by-atom, *Nature Reviews Physics* **1**, 703–715 (2019).
- [44] Y. Chen, Y. Bae, and A. J. Heinrich, Harnessing the quantum behavior of spins on surfaces, *Advanced Materials* **35**, 10.1002/adma.202107534 (2022).
- [45] R. Toskovic, R. van den Berg, A. Spinelli, I. S. Eliens, B. van den Toorn, B. Bryant, J.-S. Caux, and A. F. Otte, Atomic spin-chain realization of a model for quantum criticality, *Nature Physics* **12**, 656–660 (2016).
- [46] A. Spinelli, B. Bryant, F. Delgado, J. Fernández-Rossier, and A. F. Otte, Imaging of spin waves in atomically designed nanomagnets, *Nature Materials* **13**, 782–785 (2014).
- [47] C. Zhao, G. Catarina, J.-J. Zhang, J. C. G. Henriques, L. Yang, J. Ma, X. Feng, O. Gröning, P. Ruffieux, J. Fernández-Rossier, and R. Fasel, Tunable topological phases in nanographene-based spin-1/2 alternating-exchange Heisenberg chains, *arXiv e-prints*, arXiv:2402.13590 (2024), arXiv:2402.13590 [cond-mat.mtrl-sci].
- [48] C. Zhao, L. Yang, J. C. G. Henriques, M. Ferri-Cortés, G. Catarina, C. A. Pignedoli, J. Ma, X. Feng, P. Ruffieux, J. Fernández-Rossier, and R. Fasel, Gapless spin excitations in nanographene-based antiferromagnetic spin-1/2 Heisenberg chains, *arXiv e-prints*, arXiv:2408.10045 (2024), arXiv:2408.10045 [cond-mat.mtrl-sci].
- [49] X. Su, Z. Ding, Y. Hong, N. Ke, K. Yan, C. Li, Y. Jiang, and P. Yu, Fabrication of Spin-1/2 Heisenberg Antiferromagnetic Chains via Combined On-surface Synthesis and Reduction for Spinon Detection, *arXiv e-prints*, arXiv:2408.08801 (2024), arXiv:2408.08801

- [cond-mat.mes-hall].
- [50] K. Sun, N. Cao, O. J. Silveira, A. O. Fumega, F. Hanindita, S. Ito, J. L. Lado, P. Liljeroth, A. S. Foster, and S. Kawai, Heisenberg Spin-1/2 Antiferromagnetic Molecular Chains, [arXiv e-prints](#), [arXiv:2407.02142 \(2024\)](#), [arXiv:2407.02142 \[cond-mat.mes-hall\]](#).
- [51] Z. Yuan, X.-Y. Zhang, Y. Jiang, X. Qian, Y. Wang, Y. Liu, L. Liu, X. Liu, D. Guan, Y. Li, H. Zheng, C. Liu, J. Jia, M. Qin, P.-N. Liu, D.-Y. Li, and S. Wang, Atomic-Scale Imaging of Fractional Spinon Quasiparticles in Open-Shell Triangulene Spin- $\frac{1}{2}$ Chains, [arXiv e-prints](#), [arXiv:2408.08612 \(2024\)](#), [arXiv:2408.08612 \[cond-mat.mtrl-sci\]](#).
- [52] S. Mishra, G. Catarina, F. Wu, R. Ortiz, D. Jacob, K. Eimre, J. Ma, C. A. Pignedoli, X. Feng, P. Ruffieux, J. Fernández-Rossier, and R. Fasel, Observation of fractional edge excitations in nanographene spin chains, *Nature* **598**, 287–292 (2021).
- [53] H. Wang, P. Fan, J. Chen, L. Jiang, H.-J. Gao, J. L. Lado, and K. Yang, Construction of topological quantum magnets from atomic spins on surfaces, *Nature Nanotechnology* **10.1038/s41565-024-01775-2** (2024).
- [54] C. Peng, L. Zhang, and Z.-Y. Lu, Deconfined quantum phase transition of a higher-order symmetry-protected topological state, *Phys. Rev. B* **104**, 075112 (2021).
- [55] Y. You, T. Devakul, F. J. Burnell, and T. Neupert, Higher-order symmetry-protected topological states for interacting bosons and fermions, *Phys. Rev. B* **98**, 235102 (2018).
- [56] O. Dubinkin and T. L. Hughes, Higher-order bosonic topological phases in spin models, *Phys. Rev. B* **99**, 235132 (2019).
- [57] J. Bibo, I. Lovas, Y. You, F. Grusdt, and F. Pollmann, Fractional corner charges in a two-dimensional superlattice Bose-Hubbard model, *Phys. Rev. B* **102**, 041126 (2020).
- [58] H. Song, S.-J. Huang, L. Fu, and M. Hermele, Topological Phases Protected by Point Group Symmetry, *Phys. Rev. X* **7**, 011020 (2017).
- [59] J. Wang, X.-G. Wen, and E. Witten, Symmetric Gapped Interfaces of SPT and SET States: Systematic Constructions, *Phys. Rev. X* **8**, 031048 (2018).
- [60] T. Yoshida, T. Morimoto, and A. Furusaki, Bosonic symmetry-protected topological phases with reflection symmetry, *Phys. Rev. B* **92**, 245122 (2015).
- [61] B. Zeng, X. Chen, D.-L. Zhou, and X.-G. Wen, Symmetry-Protected Topological Phases, in *Quantum Information Meets Quantum Matter* (Springer New York, 2019) p. 281–332.
- [62] T. Kariyado, T. Morimoto, and Y. Hatsugai, Z_N Berry Phases in Symmetry Protected Topological Phases, *Phys. Rev. Lett.* **120**, 247202 (2018).
- [63] S. Takayoshi, P. Pujol, and A. Tanaka, Field theory of symmetry-protected valence bond solid states in (2+1) dimensions, *Phys. Rev. B* **94**, 235159 (2016).
- [64] L. Zhang and F. Wang, Unconventional Surface Critical Behavior Induced by a Quantum Phase Transition from the Two-Dimensional Affleck-Kennedy-Lieb-Tasaki Phase to a Néel-Ordered Phase, *Phys. Rev. Lett.* **118**, 087201 (2017).
- [65] X. Chen, Z.-X. Liu, and X.-G. Wen, Two-dimensional symmetry-protected topological orders and their protected gapless edge excitations, *Phys. Rev. B* **84**, 235141 (2011).
- [66] X.-G. Wen, Colloquium: Zoo of quantum-topological phases of matter, *Rev. Mod. Phys.* **89**, 041004 (2017).
- [67] P. Willke, Y. Bae, K. Yang, J. L. Lado, A. Ferrón, T. Choi, A. Ardavan, J. Fernández-Rossier, A. J. Heinrich, and C. P. Lutz, Hyperfine interaction of individual atoms on a surface, *Science* **362**, 336–339 (2018).
- [68] K. Yang, Y. Bae, W. Paul, F. D. Natterer, P. Willke, J. L. Lado, A. Ferrón, T. Choi, J. Fernández-Rossier, A. J. Heinrich, and C. P. Lutz, Engineering the eigenstates of coupled spin-1/2 atoms on a surface, *Phys. Rev. Lett.* **119**, 227206 (2017).
- [69] K. Yang, S.-H. Phark, Y. Bae, T. Esat, P. Willke, A. Ardavan, A. J. Heinrich, and C. P. Lutz, Probing resonating valence bond states in artificial quantum magnets, *Nature Communications* **12**, 10.1038/s41467-021-21274-5 (2021).
- [70] J. Richter and J. Schulenburg, The spin-1/2 J_1 - J_2 Heisenberg antiferromagnet on the square lattice: Exact diagonalization for $N=40$ spins, *The European Physical Journal B* **73**, 117–124 (2009).
- [71] Y. Nomura and M. Imada, Dirac-type nodal spin liquid revealed by refined quantum many-body solver using neural-network wave function, correlation ratio, and level spectroscopy, *Phys. Rev. X* **11**, 031034 (2021).
- [72] W.-Y. Liu, D. Poilblanc, S.-S. Gong, W.-Q. Chen, and Z.-C. Gu, Tensor network study of the spin- $\frac{1}{2}$ square-lattice J_1 - J_2 - J_3 model: Incommensurate spiral order, mixed valence-bond solids, and multicritical points, *Phys. Rev. B* **109**, 235116 (2024).
- [73] F. Ferrari and F. Becca, Gapless spin liquid and valence-bond solid in the J_1 - J_2 Heisenberg model on the square lattice: Insights from singlet and triplet excitations, *Phys. Rev. B* **102**, 014417 (2020).
- [74] X. Qian and M. Qin, Absence of spin liquid phase in the J_1 - J_2 Heisenberg model on the square lattice, *Phys. Rev. B* **109**, L161103 (2024).
- [75] P. Sindzingre, N. Shannon, and T. Momoi, Phase diagram of the spin-1/2 J_1 - J_2 - J_3 Heisenberg model on the square lattice, *Journal of Physics: Conference Series* **200**, 022058 (2010).
- [76] G. Carleo and M. Troyer, Solving the quantum many-body problem with artificial neural networks, *Science* **355**, 602 (2017).
- [77] U. Schollwöck, The density-matrix renormalization group in the age of matrix product states, *Annals of Physics* **326**, 96 (2011), january 2011 Special Issue.
- [78] C. Roth, A. Szabó, and A. H. MacDonald, High-accuracy variational Monte Carlo for frustrated magnets with deep neural networks, *Phys. Rev. B* **108**, 054410 (2023).
- [79] C. Roth and A. H. MacDonald, [Group convolutional neural networks improve quantum state accuracy](#) (2021).
- [80] R. Rende, L. L. Viteritti, L. Bardone, F. Becca, and S. Goldt, A simple linear algebra identity to optimize large-scale neural network quantum states, *Communications Physics* **7**, 10.1038/s42005-024-01732-4 (2024).
- [81] A. Chen and M. Heyl, Empowering deep neural quantum states through efficient optimization, *Nature Physics* **10.1038/s41567-024-02566-1** (2024).
- [82] F. Vicentini, D. Hofmann, A. Szabó, D. Wu, C. Roth, C. Giuliani, G. Pescia, J. Nys, V. Vargas-Calderón, N. Astrakhantsev, and G. Carleo, NetKet 3: Machine Learning Toolbox for Many-Body Quantum Systems, *SciPost Physics Codebases* **10.21468/scipostphyscodeb.7** (2022).

- [83] Calculations were run as single GPU calculations on half a AMD MI250X each. States were first optimized at specific locations in parameter space, and later annealed to other locations using the pretrained weights to obtain a denser grid.
- [84] S. R. White, Density matrix formulation for quantum renormalization groups, *Phys. Rev. Lett.* **69**, 2863 (1992).
- [85] M. Fishman, S. R. White, and E. M. Stoudenmire, The ITensor Software Library for Tensor Network Calculations, *SciPost Phys. Codebases*, 4 (2022).
- [86] Gaps are fit to a functional form $\Delta(N) = a + b/\sqrt{N}$, as expected for linearly dispersive magnons.
- [87] The evolution of excited states in the $S_z = 1$ and $S_z = 0$ sectors is shown in the supplemental material, showing a clear peak of the ground state energy at the first order phase transition between stripe order and quantum magnet phases, and the change in the degeneracy of the ground state at the same point.
- [88] X. G. Wen, Mean-field theory of spin-liquid states with finite energy gap and topological orders, *Phys. Rev. B* **44**, 2664 (1991).
- [89] N. Read and S. Sachdev, Large- n expansion for frustrated quantum antiferromagnets, *Phys. Rev. Lett.* **66**, 1773 (1991).
- [90] G. Baskaran, Z. Zou, and P. Anderson, The resonating valence bond state and high- T_c superconductivity — a mean field theory, *Solid State Communications* **63**, 973–976 (1987).
- [91] X.-G. Wen, Quantum orders and symmetric spin liquids, *Phys. Rev. B* **65**, 165113 (2002).
- [92] M. Mambrini, A. Läuchli, D. Poilblanc, and F. Mila, Plaquette valence-bond crystal in the frustrated heisenberg quantum antiferromagnet on the square lattice, *Phys. Rev. B* **74**, 144422 (2006).
- [93] W. A. Benalcazar, B. A. Bernevig, and T. L. Hughes, Quantized electric multipole insulators, *Science* **357**, 61–66 (2017).
- [94] W. A. Benalcazar, B. A. Bernevig, and T. L. Hughes, Electric multipole moments, topological multipole moment pumping, and chiral hinge states in crystalline insulators, *Phys. Rev. B* **96**, 245115 (2017).
- [95] F. Schindler, A. M. Cook, M. G. Vergniory, Z. Wang, S. S. P. Parkin, B. A. Bernevig, and T. Neupert, Higher-order topological insulators, *Science Advances* **4**, 10.1126/sciadv.aat0346 (2018).
- [96] I. Petrides and O. Zilberberg, Higher-order topological insulators, topological pumps and the quantum Hall effect in high dimensions, *Phys. Rev. Res.* **2**, 022049 (2020).